Theoretical Survey of the Potential Energy Surface of Methyl Nitrite + Cu^+ Reaction

Lianming Zhao, Wenyue Guo,* Tianfang Yang, and Xiaoqing Lu

College of Physics Science and Technology, China University of Petroleum Dongying, Shandong 257061, PR China

Received: June 27, 2007; In Final Form: October 2, 2007

The gas-phase reaction of methyl nitrite with Cu^+ has been investigated using density functional theory. The geometries and energies of all the stationary points involved in the reaction have been investigated at the B3LYP/6-311+G(2df,2pd) level. Seven different structures of the encounter complexes could be formed when Cu^+ attacking at different electronegative heteroatoms of *trans* and *cis* conformational isomers of methyl nitrite, in which the inner oxygen attacks account for the most stable complexes. Extensive conversions could take place for these complexes converting into each other. Various mechanisms leading to the loss of NO and HNO are analyzed in terms of the topology of the potential energy surface. The reaction proceeds exclusively from the inner oxygen attachments, followed by four different mechanisms, i.e., direct dissociation, direct H abstraction, N−O activation, and C−H activation, where the former two provide direct channels for the respective losses of NO and HNO, the third one accounts for both of the losses, and C−H activation is unlikely to be important due to the energetics.

1. Introduction

Reactions of organic molecules with transition metal cations in the gas phase are of paramount interest in catalysis, biochemistry, and environmental chemistry.[1] Since the 1979 observation by Allison, Freas, and Ridge that atomic transition metal cations can activate C−C and C−H bonds in alkanes,[2] a huge number of papers have been devoted to the investigation of intrinsic binding properties and reactivities of transition $metal^+$ + organic molecule systems in the gas phase[3−8] and some reaction mechanisms, such as bond activation,[3−5] group transfer (including H-shift),[3−5] charge transfer,[9,10] remote functionalization,[11] ion/dipole mechanism,[12] and allylic mechanism,[3] have been revealed for the gas-phase organometallic chemistry. In this field, the combination of experiments and calculations has been a promising and powerful approach to these problems.

Methyl nitrite (**MN**), a kind of carcinogen and a convenient source of the methoxy radical that is very important in combustion and atmospheric chemistry,[13,14] is unique, because it has a very weak CH_3O-NO bond (42 kcal/mol),[15] which dominates its chemistry both in solution and in the gas phase. As a consequence, it may be possible to study differences in metal ion reactivity following the initial oxidative addition into this bond to form a common reaction intermediate CH_3O-M^+-NO, as opposed to differences due to the location of initial bond insertion. Accordingly, the gas-phase reactions of **MN** with a series of transition metal ions (groups 8−10: Fe^+, Co^+, Ni^+, Rh^+, Pd^+; group 11: Cu^+ and Ag^+) have been experimentally investigated and different product distributions have been found for the different metal ions, that is, the reactions with groups 8−10 metal ions gave extensive products (MH^+, MCO^+, $MOCH^+$, $MOCH_2^+$, MNO^+, $MOCH_3^+$, and $MHNO^+$) contrast to relatively simple product patterns for the chemistry of group 11 metal ions, i.e., $MOCH_2^+$ (86% for Cu^+ and 100% for Ag^+) and $MOCH_3^+$ (14% for Cu^+).[16] Although the intermediate CH_3O-M^+-NO following the weak bond insertion could be employed to rationalize all of these products,[16] it is important to know whether the peculiar CH_3O-NO bond has any other effects on the gas-phase reactions.

To understand these effects, in this article, we select the Cu^+ + **MN** reaction as a model of our theoretical study because it gave relatively simple product pattern.[16] Moreover, as a special metal ion with a ground-state electronic configuration of $4s^03d^{10}$, the intrinsic binding properties and reactivities of Cu^+ with organic molecules have attracted much attention from both theoreticians and experimentalists, because they play an important role in catalysis, environmental chemistry, and biochemistry.[10,17−22] The present study is to provide some fundamental information about the title reaction using density functional theory (DFT). This includes a detailed illustration of the Cu^+-**MN** bonding properties and all possible competing pathways of the reaction on the ground-state potential energy surface (PES).

2. Computational Details

The hybrid density functional B3LYP method[23,24] in conjunction with the 6-311+G(2df,2pd) basis set[25] was employed in the structural optimization for all the reactants, products, and intermediates involved in the title reaction. This selected method has been shown to provide both geometries and vibrational frequencies in fairly good agreement with experimental results[22,26] and for the particular case of Cu^+-containing complexes it has been tested to be free of the pathologies that affect high-level ab initio formalisms, as the G2 theory or even the CCSD(T) method is used.[27] These facts favor its application in the investigation of the reactions of Cu^+ with neutral organic molecules, such as methylamine, aromatic amino acids, phenyl derivatives, glycine, ethylenediamine, ethynylsilanes, ethynylgermanes, and ethynylamine.[1d,10,18,21,22] The harmonic vibrational frequencies of the optimized stationary points were calculated at the same level to estimate the zero point energies (ZPE) that are included in all cited relative energies and to characterize the stationary points on the PES as local minima or transition states. All energies are reported with the ZPE corrections. The ZPE scaling factor was determined to be

* Correspondence should be addressed to wyguo@hdpu.edu.cn.

10.1021/jp075007i CCC: $40.75
Published on Web 12/28/2007

TABLE 1: Bond Dissociation Energies BDE (in kcal/mol) at 0 K Determined by Calculations and Experiments

species	exp	calc[d,e]
Cu^+-H	21.2 ± 3[a]	25.1 (3.9 ± 3)
Cu^+-O	31.1 ± 2.8[b]	30.4 (-0.7 ± 2.8)
Cu^+-NO	26.1 ± 1.2[c]	27.1 (1.0 ± 1.2)
Cu^+-CO	35.5 ± 1.6[a]	36.2 (0.7 ± 1.6)
Cu^+-OCH_2	$\geq 35.6 \pm 1.9$[a]	41.3 ($\leq 5.7 \pm 1.9$)
Cu^+-CH_2	61.2 ± 1.2[a]	61.7 (0.5 ± 1.2)
Cu^+-CH_3	26.4 ± 1.6[a]	35.0 (8.6 ± 1.6)

[a] Reference 33. [b] Reference 34. [c] Reference 35. [d] The B3LYP/6-311+G(2df,2pd) level. [e] Values in parentheses are error bars of BDEs expected at the chosen levels of theory and were obtained by subtracting the experimental values from the calculated BDEs.

0.956 on the basis of a least-square fit of the B3LYP/6-311+G(2df,2pd) calculated frequencies with the experimental values of the **MN** molecule.[28] Intrinsic reaction coordinate (IRC) calculations[29] were performed to identify the pathways between the transition states and their connecting minima. To evaluate whether spin contamination can influence the quality of the calculated results, we detected the values of $\langle S^2 \rangle$ for all the calculated species and found that all of the $\langle S^2 \rangle$ deviations are negligible (see Table S1 in Supporting Information), suggesting that in all the calculations spin contamination is negligibly small. We also made use of the natural bond orbital (NBO) theory[30] to characterize the bonds and the interactions inside some important complexes. All of the calculations were carried out using the GAUSSIAN 03[31] and NBO 5.0[32] program packages.

3. Results and Discussion

In the following sections, we will first establish the accuracy that is expected from the employed level of theory for the Cu^+/**MN** system. Next, we will present the theoretical results of various encounter complexes and their transformations for the $Cu^+ +$ **MN** system. Then, we will examine the title reaction in detail, including the geometries of various stationary points and PES profiles associated with the reaction of both *trans*- and *cis*-**MN** isomers. Last, we will briefly compare our theoretical results with the experimental findings.[16]

3.1. Calibration. To evaluate the reliability of the level of theory chosen, we compare the B3LYP calculated bond dissociation energies (BDE) with experimentally known values for some relevant Cu^+-containing species.[33−35] Table 1 collects the theoretically predicted BDEs and the most reliable experimental data for these species. Given in parentheses are error bars for the BDEs calculated at the employed level of theory, which are obtained from the subtraction of the experimental values by the calculated ones. As shown in Table 1, the theoretical values agree well with the experimental findings in most cases except Cu^+-CH_3 (8.6 ± 1.6 kcal/mol). These facts validate the ability of the level of theory to describe the features of the $[Cu, N, C, O_2, H_3]^+$ PES.

3.2. Molecular Reactants and Encounter Complexes. Both *cis*- and *trans*-conformers of **MN** (*cis*- and *trans*-**MN**) have been investigated widely both experimentally[28,36] and theoretically.[37,38] In the present study, the two isomers are also optimized and the resulting structures are shown in Figure 1. Also included in the figure (in parentheses), for comparison, are selected structural parameters derived from microwave spectra[36] We can find that the calculated structures are in good agreement with the experimental results. Energetically, the *cis*-form is calculated to be only 0.2 kcal/mol more stable than the *trans*-conformer, suggesting the coexistence of the isomers in the gas phase.

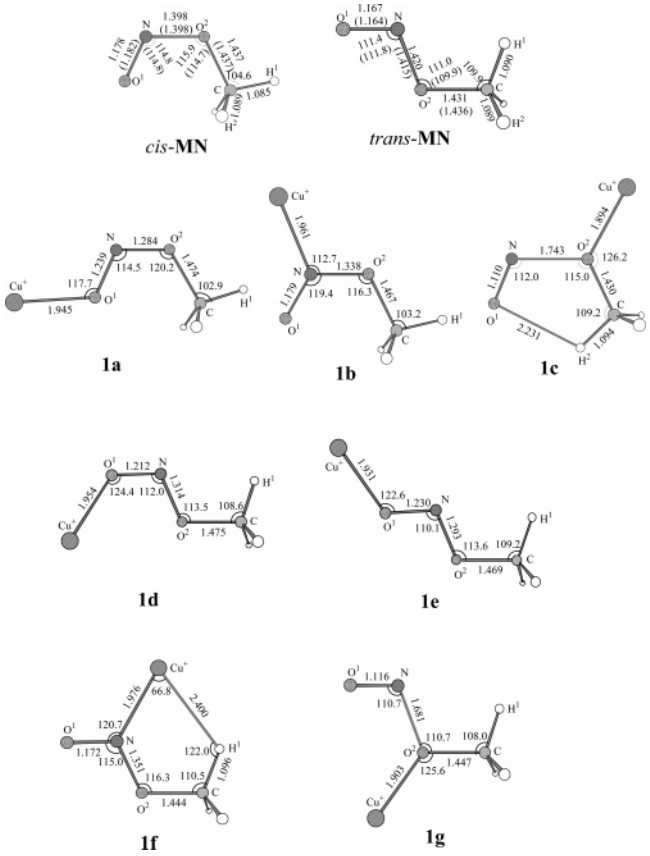

Figure 1. Optimized geometries and selected structural parameters at the B3LYP/6-311+G(2df,2pd) level for methyl nitrite, Cu^+−methyl nitrite complexes. Bond lengths are in angstroms and bond angles are in degrees.

TABLE 2: Calculated Bond Dissociation Energies BDE (in kcal/mol) of Cu^+ with Methyl Nitrite at the B3LYP/6-311+G(2df,2pd) Level of Theory

species	**1a**	**1b**	**1c**	**1d**	**1e**	**1f**	**1g**
BDE	37.5	41.3	42.3	40.2	38.8	34.4	41.9

All possible attachments of Cu^+ with **MN** are considered and seven encounter isomers, namely **1a**−**1g**, are found. Figure 1 shows the optimized geometries as well as selected structural parameters for these complexes and the relevant calculated energies are given in Table S1 together with the ZPEs and $\langle S^2 \rangle$'s. Table 2 tabulates the BDEs of Cu^+-**MN**. As shown in Figure 1, these isomers correspond to direct attachments of Cu^+ to different electronegative heteroatoms of the neutral ligands, divided either into, on the basis of the binding sites, three groups, i.e., terminal O (noted as **1a**, **1d**, **1e**), N (**1b**, **1f**), and inner O (**1c**, **1g**) attached complexes or, according to the conformations of the neutral ligands, into two groups, that is, Cu^+-*cis*-**MN** (labeled as **1a**, **1b**, **1c**) and Cu^+-*trans*-**MN** (**1d**, **1e**, **1f**, **1g**). All of the complexes have a C_s symmetry with O^1-N-O^2-C as the symmetry plane.

For *trans*-**MN**, both *trans* and *cis* terminal-O (O^1) attachments of the metal with respect to the $N-O^2$ bond (**1d** and **1e**) can be optimized due to the interaction with the different O^1 lone pairs, whereas, because of the steric effect of the methyl group, the attack of the metal at O^1 of *cis*-**MN** could only form the *trans*-association **1a**. As given in Table 2, these attachments account for the weakest and intermediate Cu^+-ligand bonds (BDE: 37.5 and 40.2−38.8 kcal/mol) among the respective *cis*- and *trans*-**MN** complexes. Upon binding to Cu^+, the largest changes in

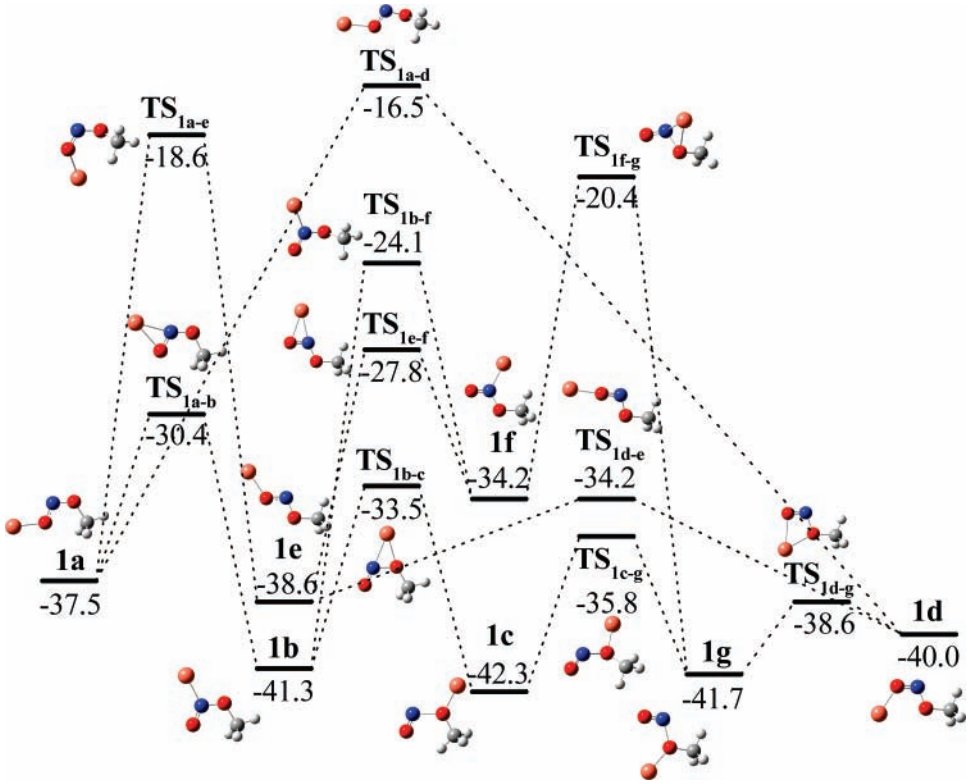

Figure 2. Energy profile for translations between the Cu^+−methyl nitrite complexes. Numbers refer to energies of the species relative to Cu^+ + *cis*-methyl nitrite evaluated at the B3LYP/6-311+G(2df,2pd) level including ZPE corrections. Scaling factor for the ZPE is 0.956. Energies are in kcal/mol.

CH_3ONO are the stretch of O^1-N bonds (by 4%−5%) and the shortening of N−O^2 bonds (by 7%−9%).

An inspection of Table 2 shows that the N attachments of Cu^+ result in the intermediate linkage (BDE: 41.3 kcal/mol) with *cis*-**MN** (**1b**) and the weakest binding (BDE: 34.4 kcal/mol) with *trans*-**MN** (**1f**). Although the attachments remarkably reinforce the N−O^2 bonds (4%-5%) and stretch the neighboring C−O^2 bonds (2%−1%), it is interesting to note that the other N−O (N−O^1) bond lengths change slightly.

It is important to note that the inner O (O^2) attachments give the strongest bindings for both the *cis*- and *trans*-**MN** complexes (BDEs: 42.3 and 41.9 kcal/mol; see Table 2). A striking structural feature of both complexes is the very large stretch of the weak O^2−N bonds (by 25% for **1c** and 18% for **1g**) and the shortening of the neighboring O^1−N bonds (by 6% and 4%). NBO analysis shows that these attachments favor strong donor−acceptor interaction from an O^1 lone pair into the σ_{O^2N}* antibonding orbital, which gives a noticeable electron population of the later bond (0.437 for **1c** or 0.375 for **1g**) and thus weakens it remarkably. This orbital interaction also results in enhancement of the electron density in the O^1-N bonding region reinforcing the linkage. It is this very strong CH_3O−NO bond activation effect that favors the direction dissociation and N−O insertion mechanisms of the Cu^+ + **MN** reaction, which will be discussed below. Furthermore, a five-member ring (O^1, N, O^2, C, H^2) structure of **1c** as shown in Figure 1 favors the direct interaction of NO with a methyl H, which would also open a new and important product channel (direct H abstraction) as will be discussed below.

3.3. Transformations between Encounter Complexes. As discussed above, attacks of Cu^+ at different basic sites of **MN** could lead to different encounter complexes. PES for the transformations among these complexes is shown in Figure 2 together with schematic geometries for the minima and transition states involved. Optimized geometries as well as selected structural parameters for the relevant transition states are given as Supporting Information (see Figure S1).

It can be found from Figure 2 that extensive conversions could take place among the encounter complexes, which can be divided into three groups, i.e., (1) transformations among the Cu^+−*cis*-**MN** complexes (**1a**, **1b**, and **1c**), which involve simple metal movements through transition states $\mathbf{TS_{1a-b}}$ and $\mathbf{TS_{1b-c}}$ with activation barriers of 7 − 11 kcal/mol; (2) those among Cu^+−*trans*-**MN** complexes (**1d**, **1e**, **1f**, and **1g**) either via simple movements of the metal (via transition states $\mathbf{TS_{1d-e}}$, $\mathbf{TS_{1e-f}}$, and $\mathbf{TS_{1d-g}}$) with activation energies between 1.4 − 11 kcal/mol or via a swing vibration of the neutral ligand through $\mathbf{TS_{1f-g}}$ with relatively higher activation barriers (13.8 kcal/mol for the **1f** → **1g** transformation and 21.3 kcal/mol for the reversal); and (3) conversions across the corresponding Cu^+−*cis*-**MN** and Cu^+−*trans*-**MN** complexes having a same binding site through simple waggles of the NO^1 group. These processes involve transition states $\mathbf{TS_{1a-d}}$, $\mathbf{TS_{1a-e}}$, $\mathbf{TS_{1b-f}}$, and $\mathbf{TS_{1c-g}}$ with energy barriers of 19 − 24 kcal/mol for the former three and ∼6 kcal/mol for the last one.

In summary, for the *cis*- and *trans*-**MN** complexes with Cu^+, the least stable encounter complexes (**1a** and **1f**) are respectively only 4.8 and 7.5 kcal/mol less stable than the most stable ones (**1c** and **1g**). Transition states for the conversions between these encounter complexes are located at 1.4−24.8 kcal/mol above the connecting minima and are much lower in energy than the separated reactants (see Figure 2). These facts suggest that all the Cu^+−**MN** complexes are experimentally accessible and could convert into each other readily.

3.4. Gas-Phase Reaction Mechanisms. Reference 16 has shown that only two neutral eliminations corresponding to HNO (major) and NO (minor) account for the gas-phase reaction of Cu^+ with **MN**. In the following sections, we shall present a

TABLE 3: Summary of All the Possible Products Associated with the Reaction of Cu^+ with Methyl Nitrite at the B3LYP/6-311+G(2df,2pd) Level of Theory

products	notations	relative energies with respect to Cu^+ + *cis*-**MN** (kcal/mol)	relative energies with respect to Cu^+ + *trans*-**MN** (kcal/mol)
Cu^+OCH_2 + HNO	**P1−1**	−27.1	−27.3
Cu^+OCH_2 + NOH	**P1−2**	13.0	12.8
Cu^+OCH_3 + NO	**P2−1**	−8.2	−8.4
HCu^+OCH_2 + NO	**P2−2**	−7.9	−8.1
$Cu^+H + CH_2O$ + NO	**P2−3**	35.0	34.9
$Cu^+NH(O) + OCH_2$	**P3−1**	−25.0	−25.1
$Cu^+HNO + OCH_2$	**P3−2**	−5.5	−5.7
$HCu^+NO + OCH_2$	**P3−3**	1.9	1.8
$Cu^+NOH + OCH_2$	**P3−4**	4.7	4.5
$Cu^+NO + OCH_3$	**P4**	7.9	7.7

systematic survey of the PES profiles for both the *cis*- and *trans*-**MN** reactions to find the reaction mechanisms. For clarification, Table 3 summarizes notations as well as relative energies with respect to the separated reactants for all the possible products associated with the reactions.

3.4.1. Reaction of Cu^+ with cis-CH_3ONO. We have considered the reaction starting from all the Cu^+−*cis*-**MN** complexes (**1a**, **1b**, and **1c**), however, only that from **1c**, the most stable *cis*-**MN** complex, could be located to give the experimentally observed products. Hence only the possible reaction pathways following formation of the complex will be discussed. Optimized geometries as well as structural parameters for all the minima and saddle points involved in the reaction are depicted in Figures 3−5 and the corresponding PES is shown in Figure 6. Calculated energies together with ZPEs and $\langle S^2 \rangle$ values are tabulated in Table S1 for all these species.

N−O Bond Activation. From Figures 3 and 6, we can find this mechanism implies an initial inner N−O ($N-O^2$) insertion of **1c** for forming complex **2**, a six-member planar ring structure (C_s), via transition state $\mathbf{TS_{1c-2}}$. Although this new species is 18.5 kcal/mol less stable than **1c** and the activation barrier for this transfer is 21.9 kcal/mol, they are both at least 20 kcal/mol more stable than the entrance channel.

Once complex **2** is formed, it could be followed by four possible channels via nonreactive dissociation, H shift-dissociation, and non-H shift-rearrangement. Different breaks of the ring constitute the first two channels which account for the direct NO and NOH elimination products Cu^+OCH_3 (**P2−3**) and Cu^+OCH_2 (**P1−2**), exothermic by 8.2 kcal/mol and endothermic by 13.0 kcal/mol with respect to the entrance channel, respectively. The third possibility involves the ring H (H^2) abstraction by the nitrosyl oxygen giving species **3** through saddle point $\mathbf{TS_{2-3}}$, which is 12.8 kcal/mol higher in energy than complex **2** but still lies at 11.0 kcal/mol below the entrance channel. A striking feature of the new complex is that Cu^+ is nearly linearly dicoordinated with the NOH and OCH_2 groups ($\angle NCu^+O^2$ = 173.6°), which was also found as intermediates for the Cu^+−formamide reaction.[22c] NBO analysis shows that this linear structure favors formaldehyde donating electron from an oxygen 2s2p mixing orbital to σ_{Cu^+N}* (ΔE: 51.8 kcal/mol) and minimizing the repulsion between the two terminal groups as well. Different dissociations of **3** would give products **P1−2** and **P3−4**, respectively, endothermic by 13.0 and 4.7 kcal/mol for the overall reactions. The last possibility initiates also with a ring-open process, but this time it involves the rupture of the O^1-H^2 bond that 8.0 kcal/mol stabilizes the system for forming $ON-Cu^+-OCH_3$ (**4**), a C_{3v} species. Transition state ($\mathbf{TS_{2-4}}$) for this process appears "early" as mirrored by comparing its structure and energy with those of its direct reactant **2**.

Nonreactive dissociations of **4** would account for products **P2−1** and **P4**, respectively, which are 8.2 kcal/mol exothermic and 7.9 kcal/mol endothermic for the overall reactions, in accordance with the experimental finding that no OCH_3 loss but the loss of NO product was formed via the reaction of Cu^+ with **MN**.[16] Another exit channel of **4** is a methyl H migration onto the metal to form species **5**, a more stable complex. This new minimum is strikingly featured by a planar structure with the metal center tricoordinated by H, NO, and OCH_2. It should be point out that such a tricoordinated minimum was also found in the decarbonylation of acetaldehyde by $^6Fe^+$ and Ni^+ and in the reaction of acetone with Ni^+ [6b,39,40] but not found for the reaction of acetaldehyde with Co^+, Cr^+, and $^4Fe^+$.[6b,c] Electronic structure theory consistently failed to find the potential minima corresponding to $M^+(H)(CH_3)(C_2H_4)$ or $M^+(H)_2(C_2H_4)$ (M = Fe, Co, and Ni).[4,41,42] Transition state $\mathbf{TS_{4-5}}$ for this possibility constitutes the highest energy barrier along the whole reaction pathway, which lies still at ∼ 9 kcal/mol below the entrance channel.

One exit of species **5** is the direct rupture of the (HCu^+OCH_2)-NO bond accounting for the final product **P2−2**, exothermic by 7.9 kcal/mol with respect to the entrance channel. The second exit is the loss of formaldehyde to produce HCu^+NO (**P3−3**), endothermic by 1.9 kcal/mol for the overall reaction. The last exit of **5** implies the shift of the hydride H that stabilizes the system by 6.2 kcal/mol producing **6**, a linearly dicoordinated $ONH-Cu^+-OCH_2$ complex, through a low-energy barrier $\mathbf{TS_{5-6}}$ (0.8 kcal/mol above **5**; see Figure 6).

Complex **6** could undergo either direct bond cleavages giving products **P3−2**, **P2−2**, and **P1−1**, exothermic by 5.5, 7.9, and 27.1 kcal/mol, respectively, with respect to $Cu^+(^1S)$ + *cis*-CH_3ONO, or a rearrangement into the very stable complex **7** (66.9 kcal/mol below the separated reactants and indeed a global minimum) by a swing of the HNO entity through transition state $\mathbf{TS_{6-7}}$, which is calculated to be 33.6 kcal/mol below the separated reactants. The new species is also featured by a nearly linear ligand−Cu^+−ligand structure with the difference that in this case the metal binds N rather than H of the HNO group. NBO analysis shows that this N binding stabilizes the species largely by strong electron donation from the 2s2p mixing orbital of N into σ_{Cu^+O}* (ΔE: 59.0 kcal/mol) as well as back-donation from a filled metal 3d orbital to $\pi^*_{NO^1}$ (ΔE: 9.7 kcal/mol). Different dissociations of **7** would account for products **P3−1** and **P1−1**, which are calculated to be exothermic by 25.0 and 27.1 kcal/mol for the overall reactions, respectively.

As shown in Figures 3 and 6, direct dissociations of the Cu^+-O bond of **5**, **6**, and **7** would produce the formaldehyde loss products HCu^+NO (**P3−3**), Cu^+HNO (**P3−2**), and $Cu^+NH(O)$ (**P3−1**), respectively, which are energetically 9.8, 2.2, and 2.1 kcal/mol less favorable than the alternative products **P2−2**, **P2−2** and **P1−1**, in accordance with the fact that no formaldehyde loss products were detected in the gas-phase experiment.[16] Furthermore, the fact that the experiment has excluded the above-mentioned NO loss partner HCu^+OCH_2 as a product of Cu^+ + **MN** reaction[16] suggests the effective competition of the **5** → **6** → **7** conversions.

C−H Bond Activation. As shown in Figures 4 and 6, the oxidative addition of Cu^+ into a C−H bond of *cis*-**MN** that destabilizes the system by as large as 39.3 kcal/mol could result in structure **8**, a C−H insertion species, through a very "late" transition state ($\mathbf{TS_{1c-8}}$) as mirrored by its structure, bearing already greatly similar to structure **8**, and its energy, lying only 1.8 kcal/mol above **8**. In this new species, the metal locates approximately above the $C-O^2$ bond. Although the rather

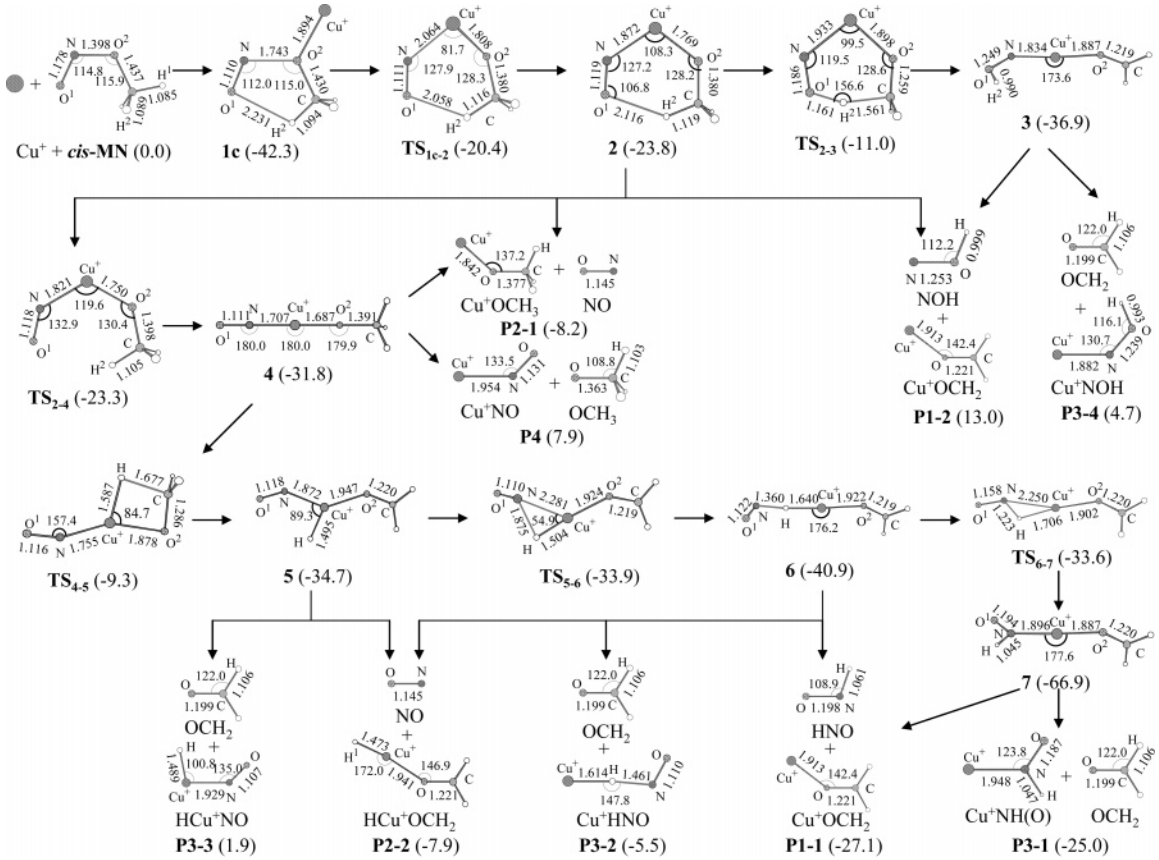

Figure 3. Reaction processes together with optimized geometries and selected structural parameters at the B3LYP/6-311+G(2df,2pd) level for species associated with the initial N−O activation pathway in the Cu^+ + *cis*-methyl nitrite reaction. The values in parentheses are energies of the species relative to the separate reactants. Bond lengths, bond angles, and energies are in angstroms, degrees, and kcal/mol, respectively.

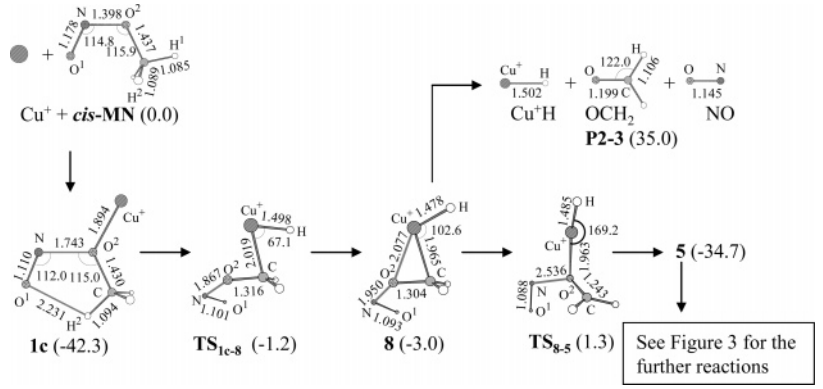

Figure 4. Reaction processes together with optimized geometries and selected structural parameters at the B3LYP/6-311+G(2df,2pd) level for species associated with the initial C−H activation pathway in the Cu^+ + *cis*-methyl nitrite reaction. Parameters follow the same notations as in Figure 3.

comparable distances of Cu^+−C and Cu^+−O^2 (1.965 and 2.077 Å, respectively), only the Cu^+−C bond is indeed formed in the complex. This situation is analogous to that found for the C−H insertion species from Cu^+−NH_2CH_3.[10] However, NBO analysis detects that in the present case Cu^+ only forms a covalent bond with H via the 4s orbital and the species is stabilized by the significant donor−acceptor interactions between Cu^+H and OCH_2 entities. Another structural feature of this species is the further activation of the N−O^2 bond, which favors a subsequent insertion into the bond by Cu^+H as will be discussed below.

Direct dissociation of **8** could produce product **P2**−**3**, endothermic by 35.0 kcal/mol for the overall reaction explaining that no such a product was found in the gas-phase reaction of Cu^+ + **MN**.[16] However, in the analogous reaction with a series of metal ions, such as Fe^+, Co^+, Ni^+, Rh^+, and Pd^+, the corresponding metal hydride ions were really found.[16] This may be because that, with respect to the BDE of CuH^+ (∼20 kcal/mol),[33,42,43] the groups 8−10 metal ions form relatively strong bonds with hydrogen (BDE: 38−50 kcal/mol).[43,44] It is expected that these larger BDE values would stabilize the hydride abstraction product as well as the C−H activation pathway, making the channel possible in the reactions of these groups 8−10 metal ions. It should be pointed out that B3LYP cannot find CH_2ONO as a stable minimum and MP2(Full)/6-311+G-(2df,2pd) also gives a very unstable species of CH_2ONO which is 37.9 kcal/mol higher in energy than OCH_2 + NO, suggesting the neutral partners of the MH^+ formation is essentially OCH_2 + NO rather than CH_2ONO as proposed by Cassady and Freiser

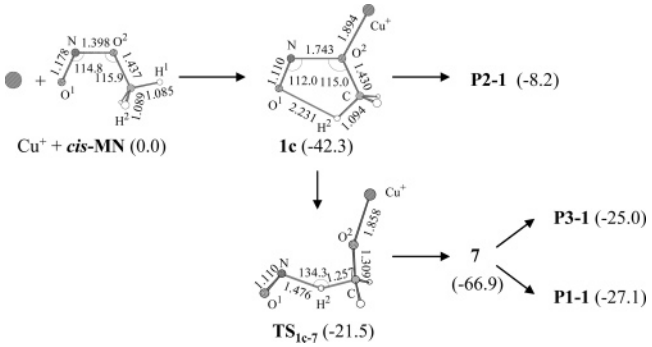

Figure 5. Reaction processes together with optimized geometries and selected structural parameters at the B3LYP/6-311+G(2df,2pd) level for species associated with the direct H abstraction and direct dissociation pathways in the Cu^+ + *cis*-methyl nitrite reaction. Parameters follow the same notations as in Figure 3.

according to thermodynamic calculations.[16] Manocha et al. also suggested that CH_2ONO formed in the reaction of CH_3ONO + F would decompose rapidly into OCH_2 + NO.[45]

Proceeding along the reaction coordinate, an extensive rearrangement for Cu^+H inserting into the weak $N-O^2$ bond would convert species **8** into complex **5**. The saddle point associated with this rearrangement ($\mathbf{TS_{8-5}}$) is found to be the most demanding point along the whole C−H activation pathway, lying 1.3 and 4.3 kcal/mol above the separated reactants and **8**, respectively. Further reactions of **5** giving various products have been discussed above.

Direct H Abstraction. In addition to the above-mentioned mechanisms, it is important to note that a direct hydrogen abstraction (H^2) by the nitrosyl nitrogen through the stretching of the $N-O^2$ bond, in which the metal ion acts just as a "spectator", could convert **1c** into complex **7** via transition state $\mathbf{TS_{1c-7}}$ (see Figures 5 and 6). Indeed, upon the attack of Cu^+ at the inner oxygen of *cis*-**MN**, strong activation of the $N-O^2$ bond is expected to take place as reflected by the lengthening of the bond length (see Figure 1). An inspection of Figure 5 shows that in $\mathbf{TS_{1c-7}}$ the $C-H^2$ bond has stretched to 1.257 Å and the $N-H^2$ bond shortened to 1.476 Å, reflecting a new HNO entity is forming. Note that this transition state is energetically 20.8 and 45.4 kcal/mol above the connected minima **1c** and **7**, or 21.5 kcal/mol below the entrance channel. These facts suggest the possibility is favorable both energetically and dynamically. As mentioned above, Nonreative dissociations of **7** would account for products **P3**−**1** and **P1**−**1**, the later of which has been observed as the major experimental product of the Cu^+ + **MN** reaction.[16]

Direct Dissociation. As discussed in section 3.2, the inner O attachment of Cu^+ results in a rather large stretch of the inner N−O bond of *cis*-**MN** (R = 1.743 Å), direct rupture of the bond giving NO + Cu^+OCH_3 (**P1**−**1**) cannot be excluded and seems to be important, because the overall reaction is exothermic by 8.2 kcal/mol (see Figures 5 and 6) and, more importantly, upon the association the N−O bond is expected to be strongly activated as reflected by the change of the bond length.

3.4.2. Reaction of Cu$^+$ + trans-CH$_3$ONO. We now turn to the reaction of Cu^+ with *trans*-**MN**. Optimized structures for the stationary points along the reaction coordinate are collected in Figures 7 and 8, and the corresponding PES is shown in Figure 9. Relevant energies for these species are also given in Table S1 together with ZPEs and $\langle S^2 \rangle$ values. As shown in Figure 9, analogous to the above-mentioned *cis* system, the reaction also generally proceeds from the most stable *trans* encounter complex, i.e., the inner O attached complex (**1g**), followed by initial N−O activation, initial C−H activation, direct H abstraction, and direct dissociation pathways.

N−O Bond Activation. As Figures 7 and 9 shows, the initial $N-O^2$ activation could lead to complex **9** through a "late" transition state $\mathbf{TS_{1g-9}}$ (lying only 0.5 kcal/mol above **9**), which has been confirmed by IRC calculations (see Figure S2).The new species indeed possesses a five-member-ring structure, in which the distances of Cu^+-N and $N-H^1$ are calculated to be 2.089 and 1.811 Å, respectively. Energetically, the species is computed to be 23.1 kcal/mol above **1g** but still lies at 18.8 kcal/mol below the entrance channel.

Once species **9** is formed, three different channels could proceed. The first pathway is the direct loss of NO accounting for product **P2**−**1**, exothermic by 8.4 kcal/mol for the overall reaction. The second one involves a rearrangement of **9** that stabilizes the system by 5.2 kcal/mol for producing complex **2**, whose reactivity has been discussed in section 3.4.1. The last one is a direct H-shift to the nitrosyl nitrogen giving the global minimum **7** through transition state $\mathbf{TS_{9-7}}$. Note that the transition state is computed to lie at 1.1 kcal/mol below **9** when ZPE corrections are included, though it is confirmed as the true first-order saddle point by IRC calculations.

C−H Bond Activation. From Figures 8 and 9, it can be found that this reaction pathway is strictly analogous to that of **1c**. Along the reaction coordinate, the metal oxidative addition into a C−H bond that destabilizes the system by as large as 37 kcal/mol could convert **1g** into species **10** (4.9 kcal/mol below the separated reactants). This possibility involves transition state $\mathbf{TS_{1g-10}}$, which lies at 1.8 kcal/mol above **10**. The structure of species **10** is analogous to that of **8** with the exception that the NO^1 entity is located *cis* with respect to O^2C. Similar to the situation of species **8**, direct dissociation of **10** could give product **P2**−**3**, lying 34.9 kcal/mol above the separate reactants. Alternatively, an extensive arrangement of Cu^+H, OCH_2, and NO groups of **10** could form intermediate **5**. This possibility involves $\mathbf{TS_{10-5}}$, which constitutes the highest energy barrier along the pathway (0.7 kcal/mol above the separated reactants). The reactivity of species **5** has been discussed in the above section.

Direct H Abstraction and Direct Dissociation. We also search for the direct H abstraction pathway for the reaction of Cu^+ with *trans*-**MN**, no any transition states can be located for this possibility. However, this channel cannot be excluded, because, as discussed above, with a simple waggle of the NO^1 group through a very low-energy barrier ($\mathbf{TS_{1c-g}}$), **1g** could convert readily into **1c**, which is then followed by the favorable and simple direct-H-abstraction pathway contributing to the neutral loss of HNO as has been discussed above.

Analogous to **1c**, the inner O attachment of Cu^+ also results in strong activation of the $ON-OCH_3$ bond in *trans*-**MN** (R = 1.681 Å), thus direct rupture of the bond giving NO + Cu^+OCH_3 (**P2**−**1**) is also favorable in the reaction of Cu^+ with the isomer (see Figure 9).

3.5. Comparison with Experimental Results. In this section, we briefly compare our theoretical results with the findings from the gas-phase experiments by Cassady and Freiser.[16] In the experiments, the reactions of **MN** with groups 8−10 metal ions, e.g., Fe^+, Co^+, Ni^+, Rh^+, and Pd^+, accounted for extensive products, such as MH^+, MCO^+, $MOCH^+$, $MOCH_2^+$, MNO^+, $MOCH_3^+$, $MHNO^+$, etc. In contrast, group 11 metal ions gave relatively simple product patterns, i.e., $MOCH_2^+$ (86% for Cu^+ and 100% for Ag^+) and $MOCH_3^+$ (14% for Cu^+). Although $MOCH_2^+$ was a common product from the reactions of the first-row groups 8−11 metal ions, H/D exchange reactions with D_2

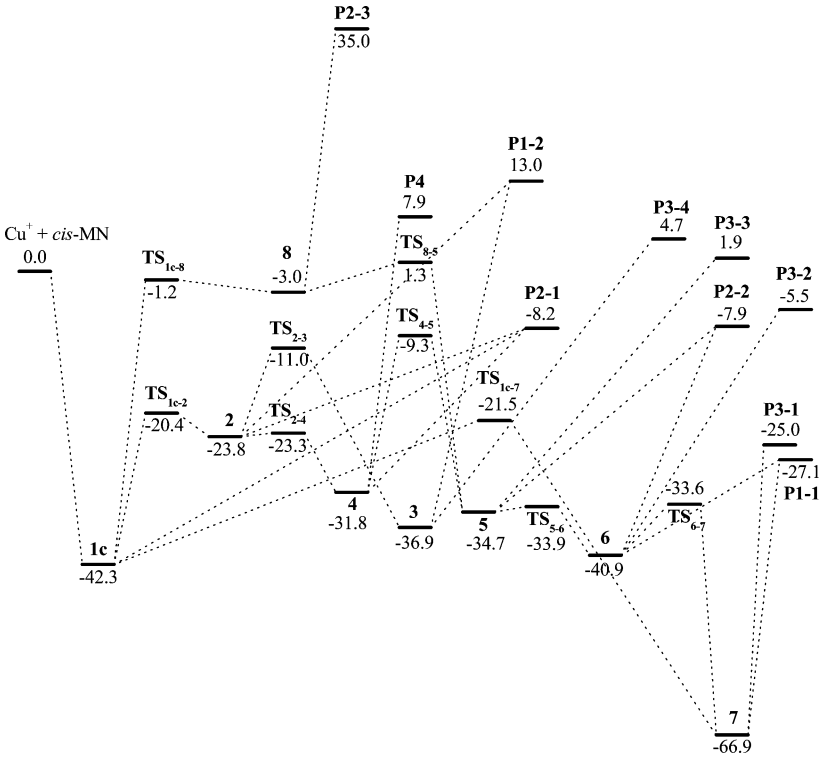

Figure 6. Energetic profile for the reaction of *cis*-methyl nitrite with Cu^+. Parameters follow the same notations as in Figure 2.

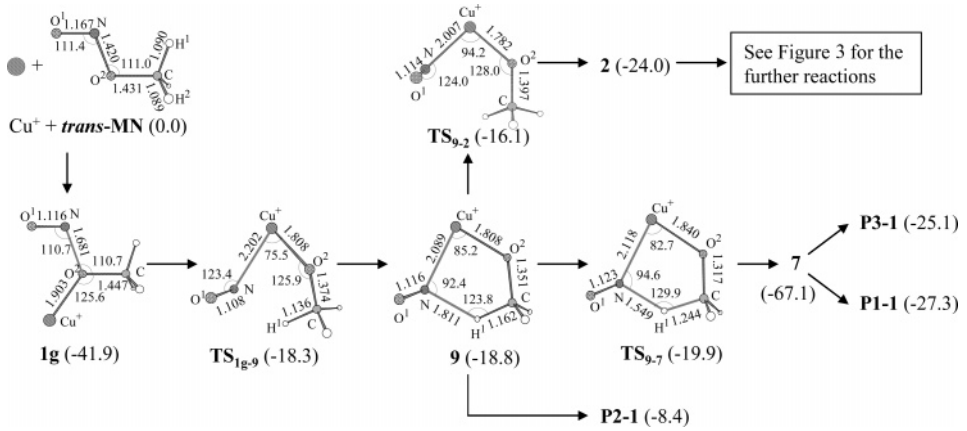

Figure 7. Reaction processes together with optimized geometries and selected structural parameters at the B3LYP/6-311+G(2df,2pd) level of theory for species associated with the initial N−O activation pathway in the Cu^+ + *trans*-methyl nitrite reaction. Parameters follow the same notations as in Figure 3.

and C_2D_4 have shown that for the reactions of Fe^+, Co^+, and Ni^+ the product ions M^+OCH_3 have equilibrating methoxy and hydrido-formaldehyde structures, whereas only the metal-methoxy structure was produced via the copper ion reaction. A same metal-insertion (into the weak CH_3O-NO bond) mechanism was invoked by the authors to rationalize the reactions of **MN** with all the metal ions.[16]

In the present theoretical investigation, although four different mechanisms, i.e., initial N−O insertion, initial C−H insertion, direct H abstraction, and direct dissociation, are found for the reaction of Cu^+ with **MN**, the initial C−H insertion mechanism seems unlikely to be important, because it experiences a relatively high-energy pathway. The hydride abstraction giving MH^+ seems to follow initial C−H activation rather than the early invoked N−O activation, though it is not produced in the Cu^+ reaction. On the other hand, direct hydrogen abstraction and direct dissociation leading respectively to the losses of HNO and NO should be important reaction mechanisms for the Cu^+ + **MN** reaction, because they are not only simple but also energetically and dynamically favorable. Furthermore, both of

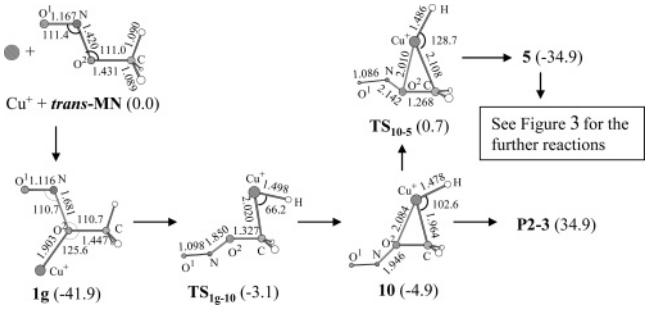

Figure 8. Reaction processes together with optimized geometries and selected structural parameters at the B3LYP/6-311+G(2df,2pd) level for species associated with the initial C−H activation pathway in the Cu^+ + *trans*-methyl nitrite reaction. Parameters follow the same notations as in Figure 3.

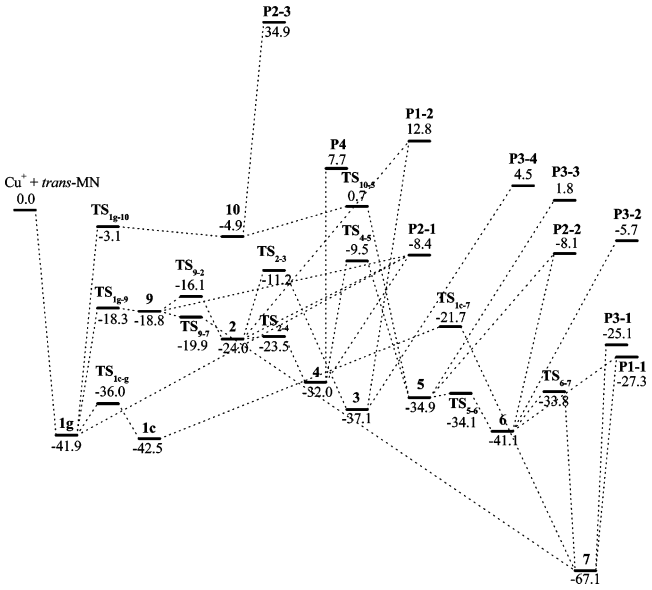

Figure 9. Energetic profile for the reaction of *trans*-methyl nitrite with Cu^+. Energies follow the same notation as in Figure 2.

the losses could also arise from the initial N−O insertion, because it also experiences an energetically favorable pathway.

4. Conclusions

This theoretical work has helped us gain further insight into the gas-phase reaction of Cu^+ with methyl nitrite. By analysis of the potential energy surface as well as comparison with the experimental findings, the reaction mechanisms appear to be uncovered. We can now conclude by summarizing a number of the main points below.

(1) Seven isomers of Cu^+-CH_3ONO complex could be formed due to direct attachments of Cu^+ with different electronegative heteroatoms (terminal O, N, and inner O) of both *cis*- and *trans*-methyl nitrite. The binding energy of these complexes is between 34 and 42 kcal/mol with the strongest bindings, among the respective *cis*- and *trans*-methyl nitrite complexes, being the inner O associations. A striking feature of the inner O attached complexes is the rather strong activation of the CH_3O-NO bond, which favors various mechanisms for the formation of the products observed experimentally.

(2) Extensive conversions could take place not only for transformations among the respective Cu^+-cis-CH_3ONO and $Cu^+-trans$-CH_3ONO complexes but also for transferring across them. All the reactions associated with the experimentally observed products start from the corresponding most stable complexes of Cu^+-cis-CH_3ONO and $Cu^+-trans$-CH_3ONO, i.e., the inner O associations, followed by initial N−O insertion, direct hydrogen abstraction, and direct dissociation mechanisms.

(3) The direct hydrogen abstraction and direct dissociation mechanisms are not only simple but also energetically and dynamically favorable; thus they should give important contributions to the respective products of HNO and NO losses in the reaction of Cu^+ with methyl nitrite.

(4) The initial N−O insertion mechanism could also account for both the experimentally observed products via the reaction of Cu^+ with methyl nitrite, because it is also energetically favorable.

(5) The initial C−H insertion mechanism is unlikely to be important for methyl nitrite reaction with Cu^+, because it experiences a relatively high-energy pathway. The hydride abstraction giving MH^+ in the reactions of methyl nitrite with first-row groups 8−10 metal ions seems to follow initial C−H activation rather than the early invoked N−O activation, though it was not observed in the Cu^+ reaction.

Acknowledgment. This work was supported by SRF for ROCS, NCET-05-0608, Excellent Young Teachers Program, and Key Project (104119) of MOE, P. R. C. National Natural Science Foundation of China (20476061), and Natural Science Foundation of Shandong Province (Y2006B35).

Supporting Information Available: Optimized geometries and selected structural parameters for transition states associated with the conversions among the encounter complexes of Cu^+-**MN**, IRC calculated results for the N−O insertion starting from the inner O attached complex of Cu^+-*trans*-**MN**, and calculated energies, zero-point energies, and $\langle S^2 \rangle$ for all the species involved in the Cu^+/**MN** reaction. This material is available free of charge via the Internet at http://pubs.acs.org.

References and Notes

(1) (a) Torrent, M.; Solà, M.; Frenking, G. *Chem. Rev.* **2000**, *100*, 439. (b) Cronin, J. R.; Chang, S. In *The Chemistry of Life's Origins*; Greenberg, J. M., Mendoza-Gómez, C. X., Pirronello, V., Eds.; Kluwer Academic Publishers: Dordrecht, The Netherlands, 1993. (c) *Metal Ions in Biological Systems*; Sigel, A., Sigel, H., Eds.; Marcel Dekker: New York, 1996; Vols. 32 and 33. (d) Corral, I.; Mó, O.; Yáñez, M. *J. Phys. Chem. A* **2003**, *107*, 1370.

(2) Allison, J.; Freas, R. B.; Ridge, D. P. *J. Am. Chem. Soc.* **1979**, *101*, 1332.

(3) Eller, K.; Schwarz, H. *Chem. Rev.* **1991**, *91*, 1121.

(4) Holthausen, M. C.; Fiedler, A.; Schwarz, H.; Koch, W. *J. Phys. Chem.* **1996**, *100*, 6236.

(5) Zhang, D. J.; Liu, C. B.; Bi, S. W.; Yuan, S. L. *Chem. Eur. J.* **2003**, *9*, 484.

(6) (a) Zhao, L. M.; Zhang, R. R.; Guo, W. Y.; Wu, S. J.; Lu, X. Q. *Chem. Phys. Lett.* **2005**, *414*, 28. (b) Zhao, L. M.; Guo, W. Y.; Zhang, R. R.; Wu, S. J.; Lu, X. Q. *ChemPhysChem* **2006**, *7*, 1345. (c) Zhao, L. M.; Zhang, R. R.; Guo, W. Y.; Lu, X. Q. *Chem. Phys. Lett.* **2006**, *431*, 56.

(7) LeCaër, S.; Mestdagh, H.; Schröder, D.; Zummack, W.; Schwarz, H. *Int. J. Mass Spectrom.* **2006**, 255−256, 239.

(8) Koo, Y. M.; Kim, T. K.; Jung, D. W.; Jung, K. W. *J. Phys. Chem. A* **2006**, *110*, 13724.

(9) Willey, K. F.; Cheng, P. Y.; Bishop, M. B.; Duncan, M. A. *Am. Chem. Soc.* **1991**, *113*, 4721.

(10) Lu, X. Q.; Guo, W. Y.; Zhao, L. M.; Chen, X. F.; Fu, Q. T.; Ma, Y. *J. Organomet. Chem.* **2007**, *692*, 3796.

(11) Lebrilla, C. B.; Schulze, C.; Schwarz, H. *J. Am. Chem. Soc.* **1987**, *109*, 98.

(12) Eller, K.; Zummack, W.; Schwarz, H. *J. Am. Chem. Soc.* **1990**, *112*, 621.

(13) (a) Wade, D.; Yang, C. S.; Metral, C. J.; Roman, J. M.; Hrabie, J. A.; Riggs, C. W.; Anjo, T.; Keefer, L. K.; Mico, B. A. *Cancer Res.* **1987**, *47*, 3373. (b) Galtress, C. L.; Morrow, P. R.; Nag, S.; Smalley, T. L.; Tschantz, M. F.; Vaughn, J. S.; Wichems, D. N.; Ziglar, S. K.; Fishbein, J. C. *J. Am. Chem. Soc.* **1992**, *114*, 1406.

(14) (a) Jonsson, A.; Bertilsson, B. M. *Environ. Sic. Technol.* **1982**, *16*, 106. (b) Wang, J.; Sun, Z.; Zhu, X. J.; Ge, M. F.; Wang, D. X. *Chem. Phys. Lett.* **2001**, *340*, 98.

(15) Patai, S. *The Chemistry of Amino, Nitroso, and Nitro Compounds and Their Derivatives*; Wiley: New York, 1982; Part 2.

(16) Cassady, C. J.; Freiser, B. S. *J. Am. Chem. Soc.* **1985**, *107*, 1566.

(17) (a) Yahiro, H.; Iwamoto, M. *Appl. Catal., A* **2001**, *222*, 163. (b) Pantazis, D. A.; Tsipis, A. C.; Tsipis, C. A. *J. Phys. Chem. A* **2002**, *106*, 1425. (c) Spoto, G.; Zecchina, A.; Bordiga, S.; Ricchiardi, G.; Martra, G.; Leofanti, G.; Petrini, G. *Appl. Catal., B* **1994**, *3*, 151. (d) Karlin, K. D.; Tyeklar, Z. *Bioinorganic Chemistry of Copper*; Chapman & Hall: New York, 1993. (e) Lippard, S. J.; Berg, J. M. *Principles of Bioinorganic Chemistry*; University Science Books: Mill Valley, CA, 1994.

(18) Hoppilliard, Y.; Ohanessian, G.; Bourcier, S. *J. Phys. Chem. A* **2004**, *108*, 9687.

(19) Taylor, W. S.; Matthews, C. C.; Parkhill, K. S. *J. Phys. Chem. A* **2005**, *109*, 356.

(20) Sklenak, S.; Hrušák, J. *J. Chem. Theory Comput.* **2006**, *2*, 997.

(21) Rimola, A.; Sodupe, M.; Tortajada, J.; Rodríguez-Santiago, L. *Int. J. Mass Spectrom.* **2006**, *257*, 60.

(22) (a) Alcamí, M.; Luna, A.; Mó, O.; Yáñez, M.; Tortajada, J. *J. Phys. Chem. A* **2004**, *108*, 8367. (b) Corral, I.; Mó, O.; Yáñez, M. *Int. J. Mass*

Spectrom. **2006**, 255−256, 20. (c) Luna, A.; Amekraz, B.; Tortajada, J.; Morizur, J. P.; Alcamí, M.; Mó, O.; Yáñez, M. *J. Am. Chem. Soc.* **1998**, *120*, 5411. (d) Galiano, L.; Alcamí, M.; Mó, O.; Yáñez, M. *ChemPhysChem.* **2003**, *4*, 72.

(23) (a) Stephens, P. J.; Devlin, F. J.; Chabalowski, C. F.; Frisch, M. J. *J. Phys. Chem.* **1994**, *98*, 11623. (b) Becke, A. D. *J. Chem. Phys.* **1993**, *98*, 5648.

(24) (a) Lee, C.; Yang, W.; Parr, R. G. *Phys. Rev. B* **1988**, *37*, 785. (b) Salahub, D. R. In *The Challenge of d and f Electrons*; Zerner, M. C., Ed.; American Chemical Society: Washington, D.C., 1989. (c) Parr, R. G.; Yang, W. *Density-Functional Theory of Atoms and Molecules*; Oxford University Press: Oxford, U.K., 1989.

(25) Frisch, M. J.; Pople, J. A.; Binkley, J. S. *J. Chem. Phys.* **1984**, *80*, 3265.

(26) Bauschlicher, C. W., Jr. *Chem. Phys. Lett.* **1995**, *246*, 40.

(27) (a) Luna, A.; Alcamí, M.; Mó, O.; Yáñez, M. *Chem. Phys. Lett.* **2000**, *320*, 129. (b) Lynch, B. J.; Truhlar, D. G. *Chem. Phys. Lett.* **2002**, *361*, 251. (c) Ghanty, T. K.; Davidson, E. R. *Int. J. Quantum Chem.* **2000**, *77*, 291.

(28) Bodenbinder, M.; Ulic, S. E.; Willner, H. *J. Phys. Chem.* **1994**, *98*, 6441.

(29) Gonzalez, C.; Schlegel, H. B. *J. Phys. Chem.* **1990**, *94*, 5523.

(30) (a) Glendening, E. D.; Reed, A. E.; Carpenter, J. E.; Weinhold, F. NBO Version 3.1. (b) Reed, A. E.; Curtiss, L. A.; Weinhold, F. *Chem. Rev.* **1988**, *88*, 899. (c) Foster, J. P.; Weinhold, F. *J. Am. Chem. Soc.* **1980**, *102*, 7211.

(31) Frisch, M. J.; Trucks, G. W.; Schlegel, H. B.; Scuseria, G. E.; Robb, M. A.; Cheeseman, J. R.; Montgomery, J. A., Jr.; Vreven, T.; Kudin, K. N.; Burant, J. C.; Millam, J. M.; Iyengar, S. S.; Tomasi, J.; Barone, V.; Mennucci, B.; Cossi, M.; Scalmani, G.; Rega, N.; Petersson, G. A.; Nakatsuji, H.; Hada, M.; Ehara, M.; Toyota, K.; Fukuda, R.; Hasegawa, J.; Ishida, M.; Nakajima, T.; Honda, Y.; Kitao, O.; Nakai, H.; Klene, M.; Li, X.; Knox, J. E.; Hratchian, H. P.; Cross, J. B.; Adamo, C.; Jaramillo, J.; Gomperts, R.; Stratmann, R. E.; Yazyev, O.; Austin, A. J.; Cammi, R.; Pomelli, C.; Ochterski, J. W.; Ayala, P. Y.; Morokuma, K.; Voth, G. A.; Salvador, P.; Dannenberg, J. J.; Zakrzewski, V. G.; Dapprich, S.; Daniels, A. D.; Strain, M. C.; Farkas, O.; Malick, D. K.; Rabuck, A. D.; Raghavachari, K.; Foresman, J. B.; Ortiz, J. V.; Cui, Q.; Baboul, A. G.; Clifford, S.; Cioslowski, J.; Stefanov, B. B.; Liu, G.; Liashenko, A.; Piskorz, P.; Komaromi, I.; Martin, R. L.; Fox, D. J.; Keith, T.; Al-Laham, M. A.; Peng, C. Y.; Nanayakkara, A.; Challacombe, M.; Gill, P. M. W.; Johnson, B.; Chen, W.; Wong, M. W.; Gonzalez, C.; Pople, J. A. *Gaussian 03*, revision B.05; Gaussian, Inc.: Pittsburgh, PA, 2003.

(32) Glendening, E. D.; Badenhoop, J. K.; Reed, A. E.; Carpenter, J. E.; Bohmann, J. A.; Morales, C. M.; Weinhold, F. *NBO 5.0.*; Theoretical Chemistry Institute: University of Wisconsin, Madison, WI, 2001.

(33) *Organometallic Ion Chemistry*; Freiser, B. S., Eds.; Kluwer: Dordrecht, The Netherlands, 1996.

(34) Rodgers, M. T.; Walker, B.; Armentrout, P. B. *Int. J. Mass Spectrom.* **1999**, *182*, 99.

(35) Koszinowski, K.; Schröder, D.; Schwarz, H.; Holthausen, M. C.; Sauer, J.; Koizumi, H.; Armentrout, P. B. *Inorg. Chem.* **2002**, *41*, 5882.

(36) Miller, S. M.; Alexander, M. H. *Chem. Phys. Lett.* **1995**, *232*, 451.

(37) Thümmel, H. T. *J. Phys. Chem. A* **1998**, *102*, 2002.

(38) Zhang, J. X.; Liu, J. Y.; Li, Z. S.; Sun, C. C. *J. Comput. Chem.* **2005**, *26*, 807.

(39) Chen, X. F.; Guo, W. Y.; Zhao, L. M.; Fu, Q. T. *Chem. Phys. Lett.* **2006**, *432*, 27.

(40) Holthausen, M. C.; Koch, W. *J. Am. Chem. Soc.* **1996**, *118*, 9932.

(41) Yi, S. S.; Blomberg, M. R. A.; Siegbahn, P. E. M.; Weisshaar, J. C. *J. Phys. Chem. A* **1998**, *102*, 395.

(42) Harrison, J. F. *Chem. Rev.* **2000**, *100*, 679.

(43) Elkind, J. L.; Armentrout, P. B. *Inorg. Chem.* **1986**, *25*, 1078.

(44) Mandich, M. L.; Halle, L. F.; Beauchamp, J. L. *J. Am. Chem. Soc.* **1984**, *106*, 4403.

(45) Manocha, A. S.; Setser, D. W.; Wickramaaratchi, M. A. *Chem. Phys.* **1983**, *76*, 129.